Published in final edited form as:
J Neurointerv Surg. 2013 November ; 5(0 3): iii33–iii37. doi:10.1136/neurintsurg-2012-010456.

Analysis and Quantification of Endovascular Coils Distribution Inside Saccular Aneurysms Using Histological Images

Hernán G. Morales[1,2], **Ignacio Larrabide**[2,1], **Arjan J. Geers**[1,2], **Daying Dai**[3], **David F. Kallmes**[3], and **Alejandro F. Frangi**[1,2,4]

[1]Center for Computational Imaging & Simulation Technologies in Biomedicine (CISTIB), Information & Communication Technologies Department, Universitat Pompeu Fabra, Barcelona, Spain.

[2]Networking Center on Biomedical Research (CIBER-BBN), Barcelona, Spain.

[3]Department of Radiology, Mayo Clinic, Rochester, MN, USA.

[4]Department of Mechanical Engineering, University of Sheffield, Sheffield, UK.

Abstract

Objective—Endovascular coiling is often performed first by placing coils along the aneurysm wall to create a frame and then by filling up the aneurysm core. However, little attention has been paid to quantify this filling strategy and to see how it changes for different packing densities. The purpose of this work is to analyze and quantify endovascular coil distribution inside aneurysms based on serial histological images of experimental aneurysms.

Method—Seventeen histological images from ten elastase-induced saccular aneurysms in rabbits treated with coils were studied. In-slice coil density, defined as the area taken up by coil winds, was calculated on each histological image. Images were analyzed by partitioning the aneurysm along its longitudinal and radial axis. Coil distribution was quantified by measuring and comparing the in-slice coil density of each partition.

Results—Mean total in-slice coil density was 22.0% ± 6.2% (range 10.1% to 30.2%). The density was non-significantly different (p=0.465) along the longitudinal axis. A significant difference (p<0.001) between peripheral and core densities was found. Additionally, peripheral-core density ratio was observed to be inversely proportional to the total in-slice coil density (R^2=0.57, p<0.001). This ratio was near unity for high in-slice coil density (around 30%).

Conclusion—Our findings demonstrate and confirm that coils tend to be located near the aneurysm periphery when few are inserted. However, when more coils are added, the radial distribution becomes more homogeneous. Coils are homogeneously distributed along the longitudinal axis.

Keywords

Experimental aneurysms; Coil density; Coil distribution; Histology

Corresponding author contact information, Hernán G. Morales: hernan.morales@upf.edu, Center for Computational Imaging & Simulation Technologies in Biomedicine (CISTIB), Information & Communications Technologies Department, Universitat Pompeu Fabra, c/Roc Boronat 138 - E08018 Barcelona – Spain. Tel: +34 93-542-1364 - Fax: +34 93-542-1451.

Competing interests
We declare that we have no competing interests.

INTRODUCTION

Endovascular coiling is often performed first by placing coils along the aneurysm wall to create a frame for succeeding coils that fill the aneurysm core.[1–5] This aneurysm filling approach from the aneurysm periphery to its core is called by some clinicians as "cocooning" occlusion technique.[1] Although this filling approach is a common clinical practice, little attention has been paid to corroborate the actual distribution of inserted coils, but most importantly, to quantify it and to see how it changes when different amount of coils are added.

The importance of studying and understanding coil distribution has to do with the post-treatment hemodynamics inside the aneurysm and ultimately in the treatment success. Previous studies reported that the hemodynamic changes after endovascular coiling depend on coil distribution inside the aneurysm.[6–9] Moreover, computational models of fluid flow with coils, which can predict the post-treatment hemodynamics, require this information to properly and accurately model the presence of the devices.[10–12]

The use of current clinical imaging techniques, such as magnetic resonance, computer tomography or digital subtracted angiography, is limited to study coil distribution. These modalities are only used to evaluate the level of aneurysm occlusion,[13] but cannot discriminate the location of individual coils inside the aneurysm. However, histological images of coiled aneurysms can provide this information. The use of induced aneurysms in animals is a feasible option to obtain such images, since they overcome the difficulties of having access to ex-vivo human aneurysm samples and, when adequately processed, distortion or destruction of the sliced tissue can be prevented.[14–16] Additionally, induced aneurysms in rabbits are similar in morphology and hemodynamic conditions to saccular cerebral aneurysms in humans, which allow us to extrapolate our findings to human aneurysm cases.[17]

The purpose of the study was to analyze and quantify coil distribution inside aneurysms using histological images of experimental coiled aneurysms. For this evaluation, the aneurysm cavity was partitioned in the longitudinal and radial orientation.

MATERIALS AND METHOD

Aneurysm Creation and Embolization Procedure

Ten New Zealand White rabbits went through a protocol approved by the animal institutional review committee at the Mayo Clinic, Rochester, Minnesota for creation of elastase-induced aneurysms followed by coil embolization. Aneurysms were created by ligation of the stump of the right common carotid artery.[15] They were allowed to mature for at least three weeks prior to embolization.[18] Aneurysms were treated with standard platinum coils as dense as possible. Before sacrifice, animals were kept alive for more than two weeks after coiling.

Tissue-Processing Procedure

Animals were deeply anesthetized and sacrificed to get access by surgery to the coiled aneurysms. Specimens were removed and immediately fixed in 10% neutral-buffered formalin for at least 24 hrs. They were then dehydrated in an ascending series of ethanol, cleared in xylene, and embedded in paraffin. Using a slow-speed diamond saw (Isomet, Beuhler, IL), 1000μm-thickness sections of the aneurysms were extracted. These sections were oriented according to the aneurysm longitudinal axis and perpendicular to the neck. Afterwards, coils were manually removed and aneurysm sections were sliced at 7μm-thickness intervals following previous cut plane. This procedure has been previously

implemented and guarantees little or no distortion of the samples.[16] Details of this process can be found elsewhere.[14–16]

A total of 17 histological images were used in this study (figure 1). For nine cases, a histological image crossing the aneurysm center was available. For six of them, a total of seven additional images away from the center were included. For last case, only an image away from the aneurysm center was available. These additional images away from the aneurysm center were included to analyze if coil density and distribution change between cut planes of the same aneurysm.

Image Processing

To evaluate coil distribution, qualitative observations and quantitative measurements were performed. For qualitative assessment, the images were visually inspected. For quantitative evaluation, the images were processed as follows.

Each image was manually processed to characterize and quantify its coil distribution. The images were processed in three steps. First, coils were manually segmented (figure 2**B**). Second, the aneurysm region containing the coils was delineated creating a closed area (blue contour in figure 2**C**). We refer to this region as the total aneurysm area. Finally, the aneurysm longitudinal axis (green line in figure 2**C**) was created by identifying the aneurysm fundus (point *f*) and neck (point *n*) on the delineated contour.

After manual processing, coil density in A_T was measured and denoted as total in-slice coil density ρ_T. Coil density is defined as the ratio between the area occupied by coils and the total area of the region:

$$\rho_x = \frac{area\ occupied\ by\ coils\ in\ region\ x}{total\ area\ of\ region\ x} \times 100\% \quad \text{(Equation 1)}$$

The aneurysm cavity was partitioned and evaluated in two ways: along its longitudinal axis, from aneurysm neck to fundus, and along its radial axis, from aneurysm periphery to its core. Both partitions generated independent regions, which were defined as follow:

Longitudinal partition: divides the aneurysm cavity into three regions along the longitudinal axis. These regions were constructed by dividing equally the longitudinal axis and were called fundus, dome and neck (figure 2**D**). The in-slice coil density of each region was calculated using equation 1 and normalized by ρ_T. The normalized densities of fundus, dome and neck were denoted as ρ_F, ρ_D and ρ_N, respectively.

Radial partition: It separates the aneurysm cavity into its periphery and core. The region within one coil diameter from the aneurysm contour was considered as the periphery, and the remaining area as the core (figure 2**D**). In-slice coil densities at peripheral and core regions were calculated using equation 1 and normalized with ρ_T. These normalized densities were denoted as ρ_P and ρ_C for peripheral and core region, respectively.

Differences between region densities were assessed with statistical tests. A Friedman's 2-way ANOVA by rank test was used to compare ρ_F, ρ_D and ρ_N, while a Wilcoxon matched-pair signed-rank test was performed to compare ρ_P and ρ_C.

Intra- and inter-observer variability on ρ_T was quantified for both coil segmentation and aneurysm delineation. For this quantification, one observer segmented and delineated all images twice to assess intra-observer variability. Inter-observer variability was evaluated by

comparing the segmentation and delineation performed by two observers of all images. The manual processing was performed independently.

RESULTS

Qualitative evaluation

From the visual inspection of the histological images (figure 3), three aspects can be highlighted. First, the aneurysm core presented large voids in some cases and coils were usually touching the aneurysm wall. Second, most coils were transversely cut resulting in circular or nearly-circular shapes. Few elongated shapes (partially longitudinal coil cuts) were visible, especially in histological samples taken from the aneurysm center. Third, from aneurysms with multiple images, it was observed that coil distribution can change from one cut plane to another.

Quantitative evaluation

After analyzing all histological images, a mean ρ_T of 22.0% ± 6.2% was found, with a minimum of 10.1% and maximum of 30.2%.

Figure 3 shows color maps of in-slice coil densities for the regions in both partitions of five images (three aneurysms). All images presented a higher ρ_P than ρ_C. Additionally, figure 3**A** and 3**e** show a homogeneous distribution of the coils (near one) along longitudinal axis with high ρ_T (>20%). Figure 3**D** has a heterogeneous distribution (low ρ_N), even though it has high ρ_T. When comparing images of same aneurysm, we observed that ρ_T can be very similar between cut planes (case #5 in figures 3**D** and 3**E**) or can change (case #4 in figures 3B and 3C).

Figure 4A depicts box plots of the normalized densities per each region. Each histological image was considered to be independent from the rest of the samples as the density depends on both coil configuration and choice of cut location.

Figure 4**B** shows the relationship between peripheral-core density ratio and ρ_T. This ratio was inversely proportional to ρ_T (R^2=0.57, p<0.001). For low ρ_T (<15%), the peripheral-core density ratio tends to be greater than 2.0 while for ρ_T around 30%, the ratio is close to 1.0.

Statistical results

The Friedman's 2-way ANOVA test showed that the differences among ρ_F, ρ_D and ρ_N were not statistically significant (p=0.465). Wilcoxon matched-pair signed-rank test reported that the difference between ρ_P and ρ_C was significant (p<0.001).

Intra- and Inter Observer variability

Mean ρ_T differences due to intra-observer variability was 0.96% ± 1.16%, ranging from 0.28% to 1.40%. Mean ρ_T differences due to inter-observer variability was 1.01% ± 1.00%, ranging from 0.05% to 0.41%.

DISCUSSION

In this work, we analyze and quantify coil distribution in saccular aneurysms using histological images to better understand this endovascular treatment. Images were obtained from elastase-induced saccular aneurysms in rabbits. These images were analyzed by partitioning the aneurysm along its longitudinal and radial axis and comparing the in-slice coil density at each region. There are three main findings.

First, coils tend to be located near aneurysm periphery when ρ_T is low (<20%). This finding confirms that the first coils produce a frame (or basket) attached to the aneurysm wall, and coils added later fill the aneurysm core.[1–3] As ρ_T increases, the peripheral-core density ratio decreases until it is close to one (figure 4**B**). This means that when more coils are added, the radial distribution tends to be more homogeneous.

Previous studies have shown that high packing density leads to better aneurysm stability after endovascular coiling.[19–22] These results might be explained by the homogeneous coil distribution that was found at high ρ_T (>25%) in this work. A homogeneous coil distribution is more likely to create a stable mechanical structure inside the aneurysm that successfully blocks and redirects the blood flow towards the parent artery. On the contrary, for low packing densities, where coils mainly lay on the aneurysm wall, leaving a hollow core, the coil structure may form a weak block against the blood flow. This hollow core at low packing densities cannot be visualized with current modalities of medical imaging. Nevertheless, this hypothesis needs to be confirmed by study the long-term treatment outcomes.

Second, densities on the longitudinal axis (fundus, dome and neck regions) were not found to be significantly different (*p*-value=0.465, Friedman's test), indicating that coils are homogeneously distributed along the aneurysm main axis.

Third, we observed that different histological images of the same aneurysm do not necessarily show similar ρ_T and coil distributions. This suggests that the characterization of in-slice coil density and distribution of a sole aneurysm should not rely on a single slide of histology, as it has been previously proposed and implemented.[23]

It has been indicated that the coil distribution inside aneurysms is random due to the limited control that clinicians have on coil deployment, and also that the distribution could be more homogeneous or uniform for certain coil shapes.[3–5] Although this "randomness" during coil deployment, our findings demonstrate that first the aneurysm periphery is filled up with coils and then its core, and also we provide evidence that coils tend to be equally distributed in the longitudinal orientation. These results clarify how coil are distributed inside the aneurysm in both axes, but most importantly, a quantification of in-slice coil density and distributions was provided.

This quantification is valuable to understand the differences that can occur among regions inside the aneurysm cavity but also it can be used to validate computational models of coils and blood flow.[10–12] The computational models need to know how coils are distributed to properly simulate the post-treatment hemodynamics inside the aneurysm. Similarly, the use of histological images and the followed methodology can be adapted to assess the porosity and strut distribution of both stents and flow diverters, and to compare it with their effect on thrombotic occlusion.[24, 25]

Recently, in-slice coil density was calculated to assess coil distribution in a similar way but in silicone coiled aneurysm models.[26] There, the authors used slices of the aneurysm dome and neck that were partitioned in angular regions to assess coil distribution. A coil uniformity index was implemented and defined as inversely proportional to the standard deviation of the in-slice coil density at each angular region. They found that a particular coil shape design has a significant higher uniformity index than the other two tested coil designs. Our results confirm this finding, since they also reported that the highest packing densities were achieved with that particular coil design. Nonetheless, this uniformity index is a relative measurement among tested coil designs.

This work has several limitations. First, the proposed methodology includes manual image processing (coil segmentation and aneurysm delineation), which introduce observer variability to our results. However, intra- and inter-variability was assessed and was not enough (around 1%) to alter our main findings and conclusions. Second, coils were removed from samples for cutting purposes, and the cast of coils induced uncertainties in some location during coil segmentation. To overcome this issue and thereby to avoid the inclusion of false-positive segmented coils, the images with doubtful coil locations were discarded from our analysis. Third, the number of cases was limited to 10 aneurysms and might not cover all possible sizes and aneurysm anatomies. Still, the number of histological images was larger (17 images) and covers a wide range of ρ_T (from 10.1% to 30.2%). Fourth, although it has been indicated that elastase-induced aneurysms in rabbits are qualitatively and quantitatively similar to those seen in large numbers of human cerebral aneurysms, [17] caution has to be taken when extrapolating our findings from experimental animal aneurysms to human cases.

CONCLUSIONS

In this work, the coil density and distribution inside the aneurysm were analyzed and quantitative evaluated using histological images of elastase-induced saccular aneurysms in rabbits treated with endovascular coils. We observed that coils are homogeneously distributed along the aneurysm longitudinal axis. Additionally, the results show that coils tend to be located near aneurysm periphery when in-slice coil density is low (<20%). As in-slice density increases, the peripheral-core density ratio decreases until it is close to one for high in-slice coil density (around 30%). This finding confirms that first coils produce a frame for succeeding coils, but also it shows that as the packing density increases, the radial coil distribution tends to be homogeneous.

Acknowledgments

Funding

The research leading to these results has received funding from the European Union Seventh Framework Programme (FP7/2007–2013) under grant agreement nr 223920, VPH-NoE project, has been partially funded by the Industrial and Technological Development Center (CDTI) under the CENIT-cvREMOD program and the Catalonian Department of Innovation, Universities and Enterprise (DIUE), through the EndoTreat project (exp. VALOR2010-00064). Alejandro F. Frangi is partially funded by the ICREA Academia programme. The animal studies were supported by Dr. Kallmes' research grants NS42646 and HL72247 from the National institute of Health in USA and by Dr. Kadirvel's grant 09SDG2160146-01 from the American Heart Association.

Reference list

1. Li MH, Gao BL, Fang C, et al. Angiographic follow-up of cerebral aneurysms treated with Guglielmi detachable coils: an analysis of 162 cases with 173 aneurysms. AJNR Am J Neuroradiol. 2006; 27(5):1107–1112. [PubMed: 16687553]
2. Pruvo JP, Leclerc X, Ares GS, Lejeune JP, Leys D. Endovascular treatment of ruptured intracranial aneurysms. J Neurol. 1999; 246(4):244–249. [PubMed: 10367691]
3. Vallee JN, Pierot L, Mont'alverne F, et al. Unruptured intracranial aneurysms treated by three-dimensional coil embolization: evaluation of the postoperative aneurysm occlusion volume. Neuroradiology. 2005; 47(6):438–445. [PubMed: 15906022]
4. Lubicz B, Leclerc X, Gauvrit JY, Lejeune JP, Pruvo JP. Three-dimensional packing with complex orbit coils for the endovascular treatment of intracranial aneurysms. AJNR Am J Neuroradiol. 2005; 26(6):1342–1348. [PubMed: 15956495]
5. Piotin M, Iijima A, Wada H, Moret J. Increasing the packing of small aneurysms with complex-shaped coils: an in vitro study. AJNR Am J Neuroradiol. 2003; 24(7):1446–1448. [PubMed: 12917143]

6. Byun HS, Rhee K. CFD modeling of blood flow following coil embolization of aneurysms. Med Eng Phys. 2004; 26(9):755–761. [PubMed: 15564112]
7. Morales HG, Kim M, Vivas EE, et al. How Do Coil Configuration and Packing Density Influence Intra-Aneurysmal Hemodynamics? AJNR Am J Neuroradiol. 2011; 32(10):1935–1941. [PubMed: 21885712]
8. Schirmer CM, Malek AM. Critical influence of framing coil orientation on intra-aneurysmal and neck region hemodynamics in a sidewall aneurysm model. Neurosurgery. 2010; 67(6):1692–1702. [PubMed: 21107200]
9. Goubergrits L, Thamsen B, Berthe A, et al. In vitro study of near-wall flow in a cerebral aneurysm model with and without coils. AJNR Am J Neuroradiol. 2010; 31(8):1521–1528. [PubMed: 20488901]
10. Cha KS, Balaras E, Lieber BB, Sadasivan C, Wakhloo AK. Modeling the interaction of coils with the local blood flow after coil embolization of intracranial aneurysms. J Biomech Eng. 2007; 129(6):873–879. [PubMed: 18067391]
11. Kakalis NM, Mitsos AP, Byrne JV, Ventikos Y. The haemodynamics of endovascular aneurysm treatment: a computational modelling approach for estimating the influence of multiple coil deployment. IEEE Trans Med Imaging. 2008; 27(6):814–824. [PubMed: 18541488]
12. Mitsos AP, Kakalis NM, Ventikos YP, Byrne JV. Haemodynamic simulation of aneurysm coiling in an anatomically accurate computational fluid dynamics model: technical note. Neuroradiology. 2008; 50(4):341–347. [PubMed: 18043912]
13. Henkes H, Fischer S, Weber W, et al. Endovascular coil occlusion of 1811 intracranial aneurysms: early angiographic and clinical results. Neurosurgery. 2004; 54(2):268–280. discussion 80-5. [PubMed: 14744273]
14. Kallmes DF, Helm GA, Hudson SB, et al. Histologic evaluation of platinum coil embolization in an aneurysm model in rabbits. Radiology. 1999; 213(1):217–222. [PubMed: 10540665]
15. Altes TA, Cloft HJ, Short JG, et al. Creation of saccular aneurysms in the rabbit: a model suitable for testing endovascular devices. American Roentgen Ray Society. Ajr. 2000; 174(2):349–354.
16. Dai D, Ding YH, Danielson MA, et al. Modified histologic technique for processing metallic coil-bearing tissue. AJNR Am J Neuroradiol. 2005; 26(8):1932–1936. [PubMed: 16155137]
17. Zeng Z, Kallmes DF, Durka MJ, et al. Hemodynamics and anatomy of elastase-induced rabbit aneurysm models: similarity to human cerebral aneurysms? AJNR Am J Neuroradiol. 2011; 32(3): 595–601. [PubMed: 21273353]
18. Fujiwara NH, Cloft HJ, Marx WF, Short JG, Jensen ME, Kallmes DF. Serial angiography in an elastase-induced aneurysm model in rabbits: evidence for progressive aneurysm enlargement after creation. AJNR Am J Neuroradiol. 2001; 22(4):698–703. [PubMed: 11290481]
19. Sluzewski M, van Rooij WJ, Slob MJ, Bescos JO, Slump CH, Wijnalda D. Relation between aneurysm volume, packing, and compaction in 145 cerebral aneurysms treated with coils. Radiology. 2004; 231(3):653–658. [PubMed: 15118115]
20. Kawanabe Y, Sadato A, Taki W, Hashimoto N. Endovascular occlusion of intracranial aneurysms with Guglielmi detachable coils: correlation between coil packing density and coil compaction. Acta Neurochir (Wien). 2001; 143(5):451–455. [PubMed: 11482694]
21. Tamatani S, Ito Y, Abe H, Koike T, Takeuchi S, Tanaka R. Evaluation of the stability of aneurysms after embolization using detachable coils: correlation between stability of aneurysms and embolized volume of aneurysms. AJNR Am J Neuroradiol. 2002; 23(5):762–767. [PubMed: 12006273]
22. Slob MJ, Sluzewski M, van Rooij WJ. The relation between packing and reopening in coiled intracranial aneurysms: a prospective study. Neuroradiology. 2005; 47(12):942–945. [PubMed: 16136261]
23. Sherif C, Bavinzski G, Dorfer C, Kanz F, Schuster E, Plenk H Jr. Computerized assessment of angiographic occlusion rate and coil density in embolized human cerebral aneurysms. AJNR Am J Neuroradiol. 2009; 30(5):1046–1053. [PubMed: 19299484]
24. Lopes D, Sani S. Histological postmortem study of an internal carotid artery aneurysm treated with the Neuroform stent. Neurosurgery. 2005; 56(2):E416. discussion E16. [PubMed: 15670395]

25. Sadasivan C, Cesar L, Seong J, et al. An original flow diversion device for the treatment of intracranial aneurysms: evaluation in the rabbit elastase-induced model. Stroke. 2009; 40(3):952–958. [PubMed: 19150864]

26. Mehra M, Hurley MC, Gounis MJ, et al. The impact of coil shape design on angiographic occlusion, packing density and coil mass uniformity in aneurysm embolization: an in vitro study. Journal of neurointerventional surgery. 2011; 3(2):131–136. [PubMed: 21990804]

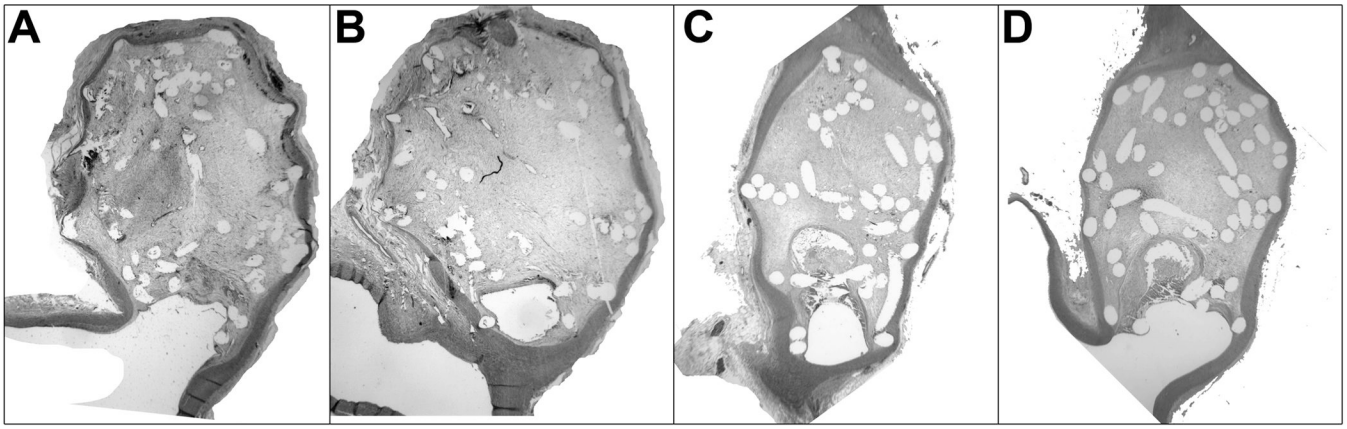

Figure 1.
Photomicrographs showing the aneurysms with removed coils. (**A**) and (**B**) correspond to case #4 (hematoxylin and eosin, original magnification, 15X) and (**C**) and (**D**) to case #5 (hematoxylin and eosin, original magnification, 20X).

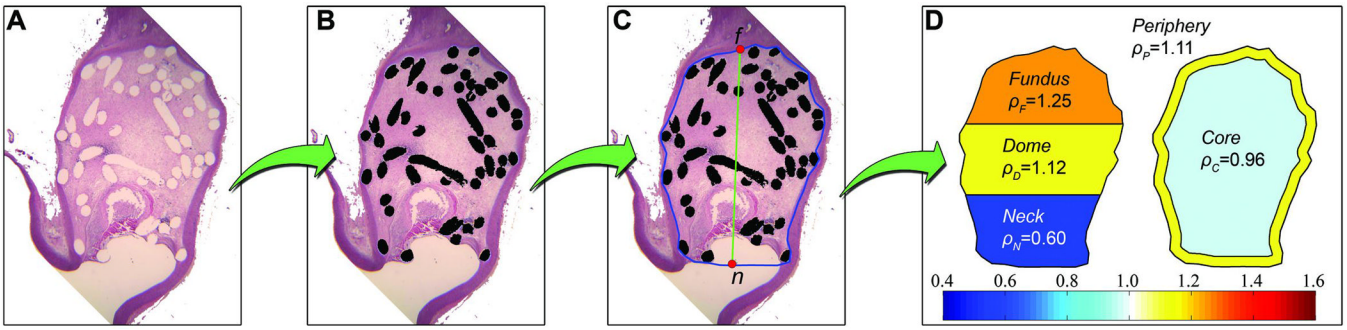

Figure 2.

Processing of a histological image. (**A**) Original histological image. (**B**) Coil segmentation. (**C**) Aneurysm wall and neck delineation (blue contour) and longitudinal axis (green line) defined by f and n (red dots). (**D**) Automatic partitioning and calculation of normalized densities.

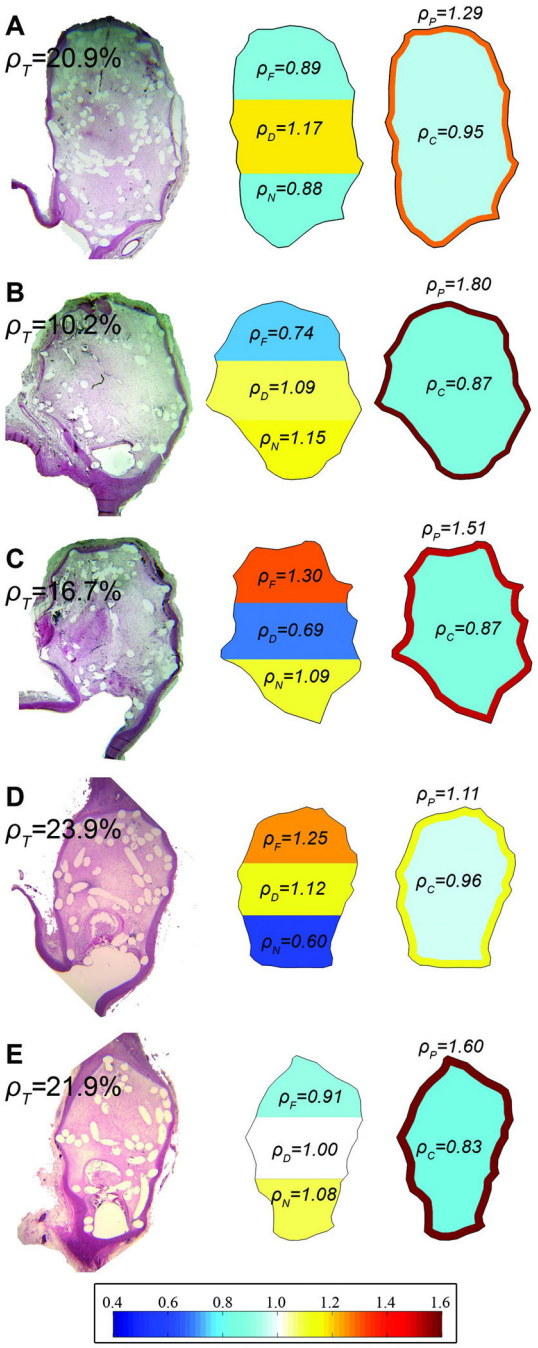

Figure 3.
Color maps of normalized coil densities for five histological images (three aneurysms).

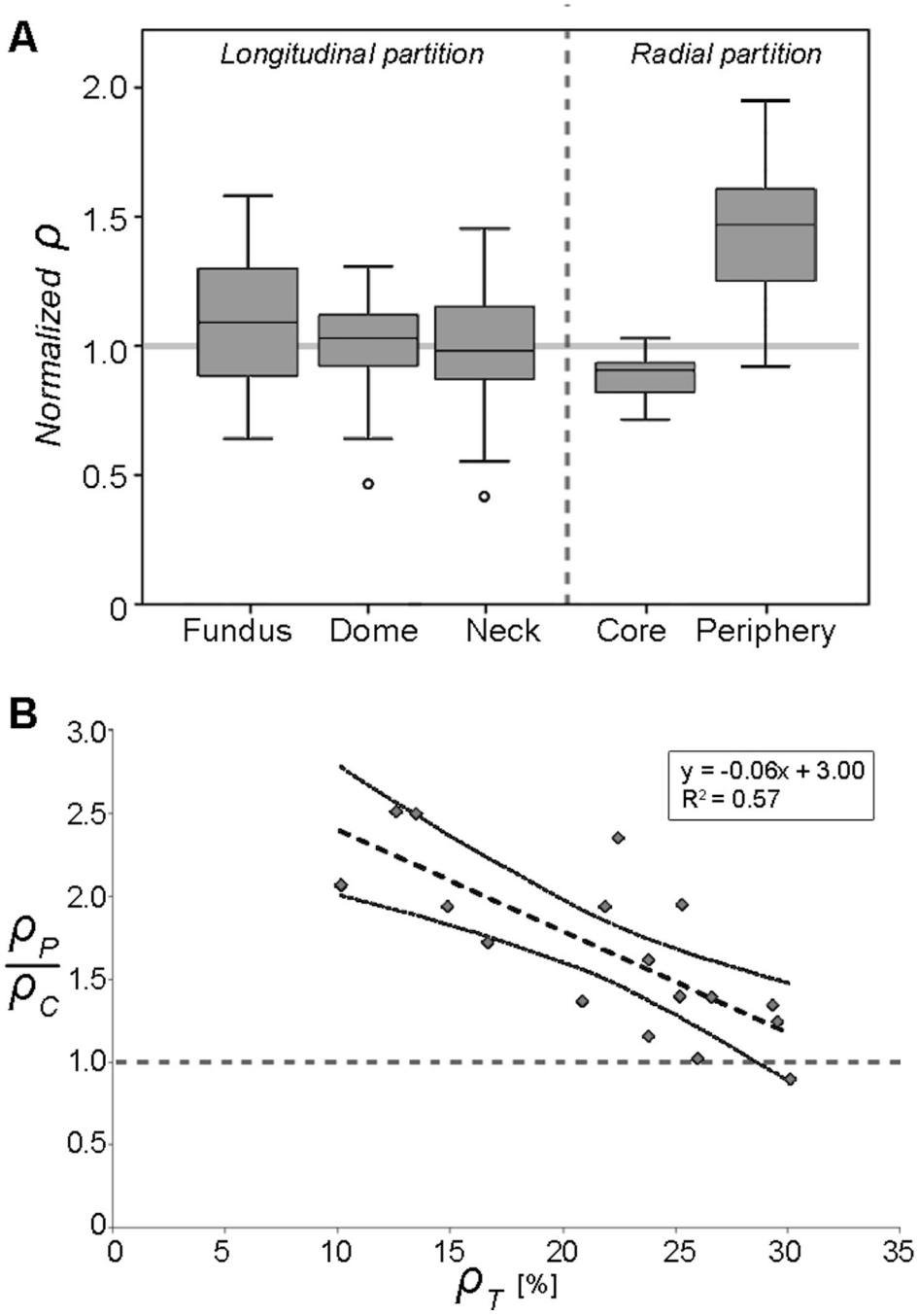

Figure 4.

(**A**) Box plot of normalized densities calculated per region. (**B**) Peripheral-core ratio versus ρ_T. Linear regression of the results is represented by the dashed line. Dotted curves are the lower and upper limits of the 95% confidence intervals.